VSP

Journal of Biomaterials Science 21 (2010) 1761–1782

Journal of BIOMATERIALS SCIENCE
brill.nl/jbs

Citric-Acid-Derived Photo-Cross-Linked Biodegradable Elastomers

Dipendra Gyawali [a,b], **Richard T. Tran** [a,b], **Kristine J. Guleserian** [c], **Liping Tang** [a,b] **and Jian Yang** [a,b,*]

[a] Department of Bioengineering, The University of Texas at Arlington, Arlington, TX 76019, USA
[b] Joint Biomedical Engineering Program, The University of Texas Southwestern Medical Center and The University of Texas at Arlington, Dallas, TX 75390, USA
[c] Division of Pediatric Cardiothoracic Surgery, Children's Medical Center, The University of Texas Southwestern Medical Center, Dallas, TX 75235, USA

Received 2 September 2009; accepted 23 October 2009

Abstract
Citric-acid-derived thermally cross-linked biodegradable elastomers (CABEs) have recently received significant attention in various biomedical applications, including tissue-engineering orthopedic devices, bioimaging and implant coatings. However, citric-acid-derived photo-cross-linked biodegradable elastomers are rarely reported. Herein, we report a novel photo-cross-linked biodegradable elastomer, referred to as poly(octamethylene maleate citrate) (POMC), which preserves pendant hydroxyl and carboxylic functionalities after cross-linking for the potential conjugation of biologically active molecules. Pre-POMC is a low-molecular-mass pre-polymer with an average molecular mass between 701 and 1291 Da. POMC networks are soft and elastic with an initial modulus of 0.07 to 1.3 MPa and an elongation-at-break between 38 and 382%. FT-IR–ATR results confirmed the successful surface immobilization of type-I collagen onto POMC films, which enhanced *in vitro* cellular attachment and proliferation. Photo-polymerized POMC films implanted subcutaneously into Sprague–Dawley rats demonstrated minimal *in vivo* inflammatory responses. The development of POMC enriches the family of citric-acid-derived biodegradable elastomers and expands the available biodegradable polymers for versatile needs in biomedical applications.

Keywords
Elastomer, photo-cross-linking, biodegradable, tissue engineering, wound dressing, citric acid

1. Introduction

Biodegradable elastomers have received significant attention for soft tissue-engineering applications due to their advantages in that they can sustain and recover

* To whom correspondence should be addressed. Tel.: (1-817) 272-0562; Fax: (1-817) 272-2251; e-mail: jianyang@uta.edu

 DOI:10.1163/092050609X12567178204169

from multiple deformations without causing irritation to the surround tissue when implanted in the body [1–6]. The mechanical irritation resulting from the compliance mismatch between implants and surround tissues has been recognized to cause significant inflammation and scar tissue formation, which ultimately prevents the implants from being effectively integrated with the surrounding tissues [7]. Among those biodegradable elastomers, recent focuses are heavily placed on cross-linked polyester elastomers such as poly(glycerol-sebacate) (PGS) and poly(diol citrates) [8–10]. It has been recognized that cross-linking confers elasticity to the polymers as similar to those naturally occurred cross-linked polymers such as collagen and elastin. PGS and poly(diol citrates) are soft and elastomeric cross-linked polyester networks and the mechanical properties of these polymers have been shown to match those of the soft tissues such as cardiac tissues and blood vessels in the body, and are, thus, considered as suitable candidate materials for soft tissue engineering [2, 9].

Photo-cross-linkable biodegradable materials have recently attracted increased attention in tissue engineering, drug delivery and wound care applications [11–24]. For tissue-regeneration applications, photo-cross-linkable biodegradable materials may be used as cell or drug carriers delivered through minimally invasive procedures [25]. Photo-cross-linkable polymers are also widely used in microfabrication for various biomedical applications such as 3-D tissue construction and cell entrapment [26, 27]. For skin graft/wound dressing applications, it is important to develop an off-the-shelf and cost-effective dressing that is able to seal irregular wounds and deliver drugs to speed the healing process [28]. Photo-cross-linkable systems may allow polymerization occurred directly in or on a tissue, thus providing advantages including localized delivery for site specific action, ease of application and a reduction in the dosage amount. Biodegradable elastomeric PGS has already been further developed into photo-cross-linkable polymers (poly(glycerol sebacate) acrylate, PGSA) by attaching acrylate groups into the PGS pre-polymer backbone to allow for free radical polymerization while still preserving elastic and biocompatible properties [29, 30]. However, the incorporation of the vinyl moiety sacrificed the pendant functionality (–OH) of the resulting polymer. It has been recognized that pendant chemistries in the bulk material are essential in order to further modify a biomaterial with biologically active molecules for targeted drug delivery or to illicit a particular cellular response [21].

Citric-acid-derived biodegradable elastomers (CABEs) such as poly(diol citrate)s, cross-linked urethane-doped polyesters (CUPE)s, elastomeric cross-linked biodegradable photoluminescent polymers (CBPLPs), poly(xylitol-co-citrate)s, etc., have recently received significant attention in various biomedical applications, including tissue-engineering orthopedic devices, bioimaging and implant coatings [31–37]. A key feature for CABEs is that citric acid acts as a robust multifunctional monomer to provide valuable pendant functionality to give the above listed polymers their unique degradation, mechanical and optical properties over existing biomaterials. Citric acid itself is an anticoagulant used in the hospital setting.

Citric acid is mainly used to participate in the ester-cross-link formation in the biomaterials, but also enhances hemocompatibility, balances the hydrophilicity of the polymer network, provides hydrogen bonding and additional binding sites for bioconjugation to confer additional functionality such as optical properties [31]. Poly(diol citrate)s have demonstrated excellent biocompatibility, including hemocompatibility for soft tissue-engineering applications [34, 38]. Poly(diol citrate)s have not been developed into a photo-cross-linkable form which still demonstrates excellent biocompatibility.

The purpose of this study was to develop a novel photo-cross-linkable biodegradable elastomer, poly(octamethylene maleate citrate)s (POMCs), based on poly(octamethylene citrate)s (POC, a representative poly(diol citrate)). This new class of synthetic polyester is composed of 1,8-octanediol (OD), maleic acid (MA) and citric acid (CA), which have all been successfully used in a wide range of biomedical applications [9, 33, 39–42]. The rationale behind the versatile POMC is (i) introducing maleate groups into the POC backbones allows for a new mode of cross-linking while preserving pendant chemistry from citrate groups for bioconjugation; (ii) POMC should preserve the previous benefits of POC, including tunable elastomeric mechanical properties, degradability and excellent biocompatibility; (iii) the synthesis should be simple and cost-effective; (iv) the low molecular mass of pre-POMC may render its injectability/processability for *in situ* applications; and (v) the cross-linking of POMC should avoid any harsh processing conditions. In the present paper, the chemical, physical and biocompatibility of POMC are studied and its potential in tissue engineering and *in situ* wound-dressing formation is also demonstrated.

2. Materials and Methods

2.1. Synthesis of Pre-POMC

All chemicals were purchased from Sigma-Aldrich and used as received. The synthesis of POMC was carried out as shown in Fig. 1. CA, OD and MA were added into a 250-ml three-necked round-bottom flask fitted with an inlet adapter and outlet adapter. The mixture was melted within 20 min by stirring the contents in the flask at a temperature of 160°C under nitrogen gas flow. Once the constituents melted, the temperature was reduced to 135°C and the reaction was allowed to progress for an additional 125 min under a nitrogen purge to create the pre-POMC. Pre-POMC was dissolved in 1,4-dioxane and precipitated in de-ionized water in order to remove any un-reacted monomers. The precipitated polymer solution was freeze-dried to obtain the purified pre-POMC. To investigate the effects of the reactant ratio on the properties of the polymer, five different MA:CA molar ratios were studied (10:0, 8:2, 6:4, 4:6 and 2:8), as shown in Table 1. The ratio of the acids over the diol for the reaction was kept as 1:1.

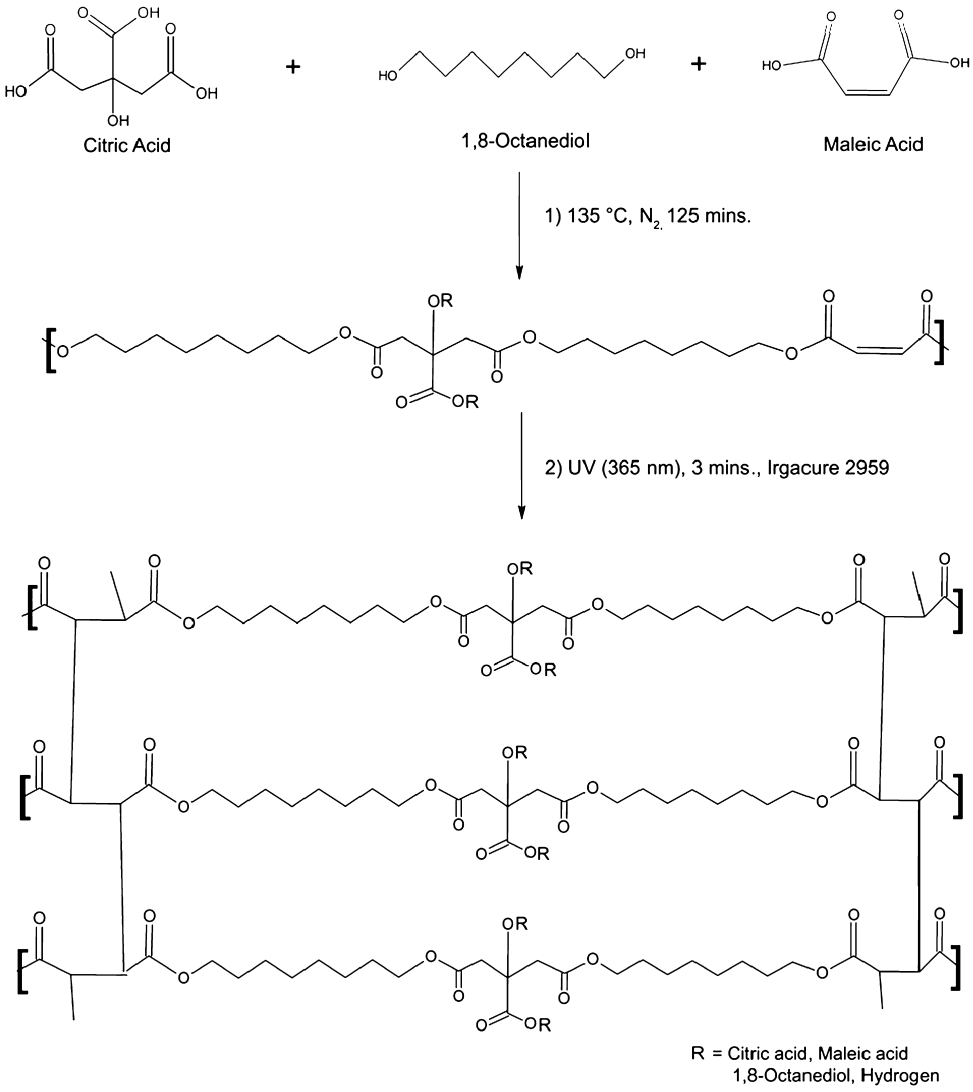

Figure 1. Schematics of POMC synthesis. Step 1: Synthesis of pre-POMC by reacting citric acid, maleic acid and 1,8-octanediol. Ratios of maleic acid and citric acid were varied as 10:0, 8:2, 6:4, 4:6 and 2:8, respectively, whereas the ratio of overall acid to diol was kept as 1:1. All the monomers were melted at 160°C under a nitrogen blanket. Further polymerization was continued at 135°C for 125 min to obtain a low-molecular-weight pre-polymer. Step 2: Photo-cross-linking of pre-POMC was performed under 365 nm UV light for 3 min in the presence of a photoinitiator (Igacure 2959).

2.2. Characterization of Pre-POMC

The weight-average molecular weight of the pre-POMCs was analyzed by an Autoflex matrix-assisted laser desorption/ionization mass spectroscope (MALDI-MS; Bruker Daltonics). 2-(4-Hydroxyphenyl-azo)-benzoic acid (HABA) was used as

Table 1.
Feeding ratio and actual composition of pre-POMC

Polymer	Composition		Feeding ratio MA:CA:OD (mol)
	MA:CA:OD (mol)	MA:CA:OD (%l)	
POMC10/0	0.10/0.00/0.10	0.51/0.0/0.49	0.5/0.0/0.50
POMC8/2	0.08/0.02/0.10	0.38/0.12/0.51	0.4/0.1/0.50
POMC6/4	0.06/0.04/0.10	0.29/0.21/0.49	0.3/0.2/0.50
POMC4/6	0.04/0.06/0.10	0.19/0.32/0.49	0.2/0.3/0.50

the matrix to mix with the pre-POMCs in a 1:1000 pre-polymer/matrix molar ratio. The functional groups present in the pre-polymers were analyzed by Fourier transform infra red (FT-IR) spectroscopy using a Nicolet 6700 FT-IR (Thermo Scientific). Pre-POMCs were dissolved in dimethyl sulfoxide-d_6 (DMSO-d_6) in a 5-mm outside-diameter tube and analyzed by ^{1}H-NMR using a 250 MHz JNM ECS 300 (Jeol). The chemical shifts for the ^{1}H-NMR spectra were recorded in parts per million (ppm), and were referenced relative to tetramethylsilane (TMS, 0.00 ppm) as the internal reference.

2.3. Preparation and Characterization of Photo-Cross-Linked POMC

Pre-POMC was cross-linked by free radical polymerization. The purified pre-polymer was dissolved in dimethylsulfoxide (DMSO) to obtain a 50% (w/w) polymer solution. To generate the free radicals, 1% (w/w) photoinitiator (PI), 2-hydroxy-1[4(hydroxyethoxy)phenyl]-2-methyl-1 propanone (Irgacure 2959), was dissolved in the polymer solvent solution. Next, the solution was poured into a Teflon mold and placed under a UVP 365 nm long-wave UV lamp (*ca.* 4 mW/cm^2, model 100AP, Blak-Ray) for 3 min. The thermoset elastomer achieved through this process is shown in Fig. 1. Photo-cross-linking of POMC2:8 with the desired amount of PI (<2.5%) was not achieved and not considered for further characterization. Bond vibrations of cross-linked film of POMC were evaluated using FT-IR spectroscopic analysis.

2.4. Thermal Characterization of Photo-Cross-Linked POMC

The thermal behavior of the cross-linked films for three different ratios of POMC was studied by differential scanning calorimetry (DSC; DSC550, Instrument Specialists) and thermogravimetric analysis (TGA; Mettler Toledo). For the DSC analysis, samples were first scanned up to 150°C at a heating rate of 10°C/min under nitrogen purge (50 ml/min) to remove any traces of water from the sample. Thereafter, the samples were rapidly cooled at a cooling rate of 40°C/min to −60°C. The samples were scanned again for the second time up to 230°C at a heating rate of 10°C/min. The glass-transition temperature (T_g) was determined as the middle of the recorded step change in heat capacity from the second heating run. Similarly, TGA thermograms were observed under a flow of nitrogen gas (50 ml/min)

at a scanning speed of 101°C/min in the range of 50–600°C. The decomposition temperature (T_d) was defined as the temperature at which 10% weight loss of the samples occurred.

2.5. Mechanical Properties of Photo-Cross-Linked POMC

The tensile mechanical properties were studied according to the ASTM D412a standard on an MTS Insight II mechanical tester equipped with a 500 N load cell (MTS). POMC films were cut using a dog-bone-shaped aluminum die (26 mm × 4 mm × 1.5 mm; length × width × thickness). The dog-bone-shaped films were pulled until failure at a rate of 500 mm/min to obtain the stress–strain curves. The initial slope (0–10%) of the curve was used to determine the initial modulus of the material. A detailed study on the effect of different ratios of the monomers, the amount of PI and concentration of the polymer in solvent on the mechanical properties of the polymer was performed. The density was measured using a Mettler Toledo balance equipped with a density determination kit based on Archimedes' principle.

2.6. Swelling Ratio and Sol–Gel Fraction Measurements

POMC was fabricated according to the process mentioned above. Six polymer discs (7 mm in diameter) were cut from the cross-linked films using a cork borer. The discs were weighed to find the initial mass (M_i). DMSO was used as the swelling and sol-dissolving agent in this study. Swelling studies were also conducted in PBS (pH 7.4 at 37°C). The discs were allowed to swell in the respective swelling agents until the equilibrium state was achieved. The surface of the swollen discs was gently blotted with filter paper to remove any excess swelling agent, and the sample was then weighed (M_w). The discs were freeze-dried for 3 days and weighed to determine the dry weight (M_d). The equilibrium swelling ratio was calculated using equation (1) [43]. The experiment was repeated three times and the average value was reported.

$$\text{Swelling } (\%) = \left(\frac{M_w - M_d}{M_d} \right) \times 100. \tag{1}$$

The sol–gel fraction was calculated using equation (2) [43]:

$$\text{Sol } (\%) = \left(\frac{M_i - M_d}{M_i} \right) \times 100. \tag{2}$$

2.7. In Vitro *Degradation Study*

Six polymer discs (7 mm in diameter and 3 mm in thickness) were cut from the cross-linked films using a cork borer. The discs were weighed to find the initial mass (M_i), and suspended in PBS (pH 7.4) and maintained at 37°C. The pH was monitored and the buffer was replaced every day for first week and every subsequent week to ensure a constant pH of 7.4. At the desired time point, the samples were

rinsed with de-ionized water, freeze-dried and weighed to find the remaining mass (M_t). The percent mass loss was calculated using equation (3).

$$\text{Mass loss } (\%) = \left(\frac{M_0 - M_t}{M_0} \right) \times 100. \quad (3)$$

2.8. Collagen Immobilization

POMC8/2 films (7 mm diameter, 1 mm thick) were washed by refluxing in anhydrous ethanol for 3 h and dried under vacuum. Next, the films were immersed into 10 ml of a 5 mM 2(N-morpholino)ethanesulfonic (MES) buffer solution (pH 4.5). Carboxylic acids groups were subsequently activated with 9.3 mg EDC and 3 mg NHS for 2 h with mild magnetic stirring at 4°C. Additionally, 1.5 ml of a 10 mg/ml collagen hydrochloride solution was prepared in 20 ml of a 5 mM MES solution. The activated carboxylic acid group containing films were washed twice with the 5 mM MES solution, merged into the collagen solution and gently agitated for 6 h at 4°C. Finally, the films were taken out, washed twice with de-ionized water and dried by lyophilization.

2.9. In Vitro *Cell Attachment*

POMC8/2 was used a representative polymer for all cytotoxicity evaluation studies. Photo-cross-linked and collagen-immobilized POMC films were cut into disks (7 mm diameter, 2 mm thick) and sterilized in ethanol for 30 min, and placed under UV light for another 30 min. NIH-3T3 fibroblasts (ATCC) and human aortic smooth muscle cells (HASMC, ATCC) were seeded on the surface of the polymer disks with a seeding density of 3×10^5 cells/ml. The cells were allowed to proliferate in Dulbecco's modified Eagle's medium (DMEM) with 10% fetal bovine serum (FBS) for 3 days in an incubator maintained at 37°C, 5% CO_2 and 95% humidity. The cells were then observed under an inverted microscope (Zeiss Auxiovert). A methylthiazoletetrazolium (MTT) cell proliferation and viability assay was used for a quantitative assessment of the cell growth and proliferation on POMC films and collagen-immobilized POMC films. Un-modified poly(L-lactic acid) (PLLA, 99 kDa) films were used as a control. Six discs (7 mm) of each film were cut and placed into 96-well plates. HASMCs were seeded on each of the film according to the seeding protocol mentioned above. MTT assay analysis was performed at three time-points (2, 5 and 7 days) as per the manufacturer's protocol. An Infinite200 microplate reader (Tecan Group) was used at 570 nm with a reference wavelength of 690 nm for absorbance analysis.

2.10. In Vivo *Host Response*

Cross-linked POMC8/2 discs (7 mm diameter, 2 mm thick) were fabricated and sterilized according to the procedure described as mention elsewhere [35]. The sol content of the films was removed before implantation. The discs were then implanted in 7-week-old female Sprague–Dawley rats by blunt dissection under deep isoflurane-O_2 general anesthesia. Animals were cared for in compliance with the

regulations of the Animal Care and Use Committee of The University of Texas at Arlington. POMC samples were implanted symmetrically on the upper and lower back of the same animal. The rats were killed and tissue-samples surrounding the implants were harvested with an intact implant at 1 week and 4 weeks. Samples and surrounding tissue were frozen in OCT embedding media (Polysciences) at −80°C, sectioned and H&E stained for histological evaluation. Images were taken at 10× magnification using a Leica DMLP microscope fitted with a E500 camera (Nikon). The line tool in the ImageJ Analysis Software was used to measure the thickness of the fibrous capsule. Readings from 50 random portions of each image were collected, and the averaged value was reported.

2.11. *POMC Scaffold Fabrication and* In Situ *Film Formation on Porcine Skin Cavities*

Scaffold sheets were fabricated using Teflon molds. POMC8/2 pre-polymer and PI were dissolved in 1,4-dioxane to form a 30% solution. Sieved salt (150–250 μm) was added in a 1:9 pre-polymer/salt weight ratio to form a thick slurry, and cast into the Teflon mold. After solvent evaporation, the mold was placed under a UV lamp, and then transferred into an oven maintained at 80°C for a period of 24 h. The salt was removed by leaching in de-ionized water for a period of 72 h with water changed every 6 h. The scaffolds obtained after leaching were freeze-dried for 48 h to remove all traces of water. The scaffold was then freeze fractured using liquid nitrogen, and the cross-section of the fractured sample was examined under a scanning electron microscope (SEM; S-3000N, Hitachi). For *in situ* film formation, pre-POMC8/2 and PI were mixed directly and then injected in the cavities created on porcine skin purchased from the local Wal-Mart followed by exposing under UV for 5 min.

2.12. *Statistical Methods*

All the experiments were repeated three times and the average value was reported. Data are expressed as means ± standard deviation. Statistical analysis was performed using one-way ANOVA with post hoc Neuman–Keuls testing to examine statistical difference. The swelling data and mechanical properties of the polymer were compared with one-way ANOVA. Data were taken to be significant when a P-value of 0.05 or less was obtained.

3. Results

3.1. *Structural Characterization of pre-POMC and Photo-Cross-Linked POMC*

The weight-average molecular mass of pre-POMC was measured by MALDI-MS (Fig. 2A). The peaks from the main distribution and all the sub-distributions were taken in consideration in the calculation of the weight-average molecular weight of the pre-polymer. These spectra confirmed that a low-molecular-mass pre-polymer

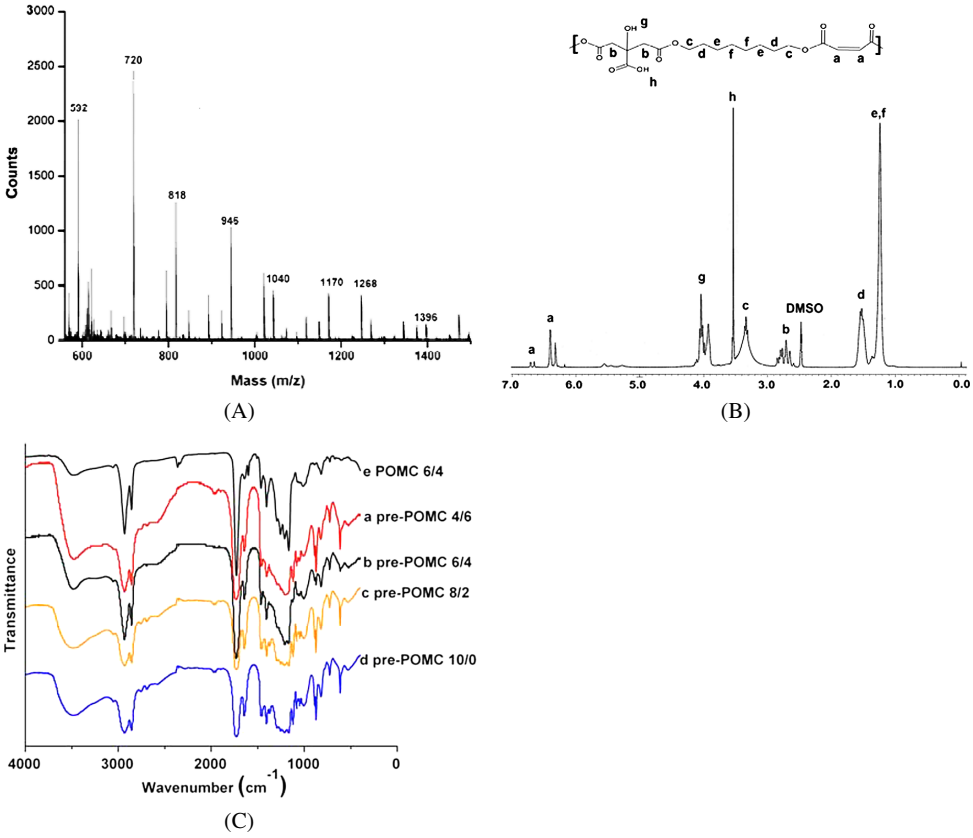

Figure 2. Structural characterization of pre-POMC. (A) MALDI-MS spectra of pre-POMC8/2. (B) ^{1}H-NMR spectra of pre-POMC8/2. (C) FT-IR spectra of pre-polymers: (a) pre-POMC4/6, (b) pre-POMC6/4, (c) pre-POMC8/2 and (d) pre-POMC 10/0. This figure is published in colour in the online edition of this journal, that can be accessed *via* http://www.brill.nl/jbs

was synthesized with a weight-average molecular mass in the range of 701 to 1291 Da (Table 2).

A typical ^{1}H-NMR spectrum of POMC8/2 can be seen in Fig. 2B. Peak (d), located at 1.53 ppm, was assigned to –O–$CH_2\underline{CH_2}$– from 1,8-octanediol [9]. Peak (b), located at 2.79 ppm, was assigned to –$C\underline{H_2}$– from citric acid [9]. The peaks located between 6 and 7 ppm were assigned to the protons of –$C\underline{H}$=$C\underline{H}$– incorporated into the polymer chain [44]. The actual composition of the pre-polymers was calculated based on the integration of the area under the characteristic proton peaks from each monomer: diol (d/4), CA (b/4) and MA (a/2). The actual polymer composition can be well controlled by varying the feeding ratio of the monomers as shown in Table 1.

Purified pre-POMC and POMC films were characterized by FT-IR as shown in Fig. 2C. The pronounced peaks at 1690–1750 cm^{-1} suggest the presence of carbonyl (C=O) groups from the ester bond and pendent carboxylic acid from the

Table 2.
Characterization of photo-cross-linked POMC polymer films

Sample	Density (g/cm^3)	Initial modulus (MPa)	Tensile strength (MPa)	Elongation (%)	Average molecular mass of pre-POMC (Da)	PDI
POMC (10/0)	1.13 ± 0.01	0.48 ± 0.07	0.29 ± 0.07	55.02 ± 9.62	1291	1.33
POMC (8/2)	1.12 ± 0.01	1.06 ± 0.11	0.88 ± 0.13	72.63 ± 7.74	874	1.38
POMC (6/4)	1.09 ± 0.01	0.28 ± 0.05	0.55 ± 0.06	169.49 ± 36.57	769	1.22
POMC (4/6)	1.08 ± 0.01	0.07 ± 0.01	0.37 ± 0.07	322.09 ± 57.95	701	1.25

Values are reported as the mean $\pm$ standard deviation ($n = 6$).

citric acid [9]. The shoulder peak of a lower wavelength at 1650 cm^{-1} proves the presence of the olefin moiety [45] from maleic acid. Similarly, the peak centered at 2931 cm^{-1} is evidence of the methylene groups from 1,8-octanediol [9]. Hydrogen-bonded hydroxyl functional groups showed absorbance as a broad peak centered at 3570 cm^{-1} on both the pre-polymer spectra and photo-cross-linked film spectra. A shoulder peak at 1647 cm^{-1} due to C=C stretching exhibits higher absorbance in pre-POMC6/4 as compared to the POMC6/4 photo-polymerized film, which indicates the reduction of the olefin moiety in the free radical polymerization cross-linking process. Similarly, the peak located at 869 cm^{-1}, which was found only in the pre-POMC, denotes the out-of-plane C–H bending of the conjugated olefin moieties.

3.2. Thermal Characterization of Photo-Cross-Linked POMC

The glass transition temperature (T_g) of the POMC films was analyzed by DSC. No crystallization or melting temperatures were observed in the thermograph. As seen in Fig. 3A, the T_g values of all the pre-polymers were below 0°C, which indicated that all the polymers are amorphous at body temperature. The T_g of POMC4/6 was as high as −9°C. POMC10/0 had the lowest T_g (−36°C). Thus, the results from Fig. 3A show that as the amount of maleic acid was increased, the T_g of the polymer was decreased. The thermal stability of POMC was analyzed by TGA. Figure 3B graphically depicts the decomposition of the polymer as the temperature was increased. POMC4/6 exhibits 10% decomposition at 363°C, whereas POMC10/0 displayed 10% decomposition at 310°C. These results confirm that as the amount of maleic acid is decreased, the polymer gains more thermal stability.

3.3. Mechanical Properties of Photo-Cross-Linked POMC

Tensile mechanical tests on POMC samples showed that as the amount of maleic acid decreased, the elastomers became softer and more elastic (Table 2). However, when no citric acid was used in the synthesis, a lower value for initial modulus

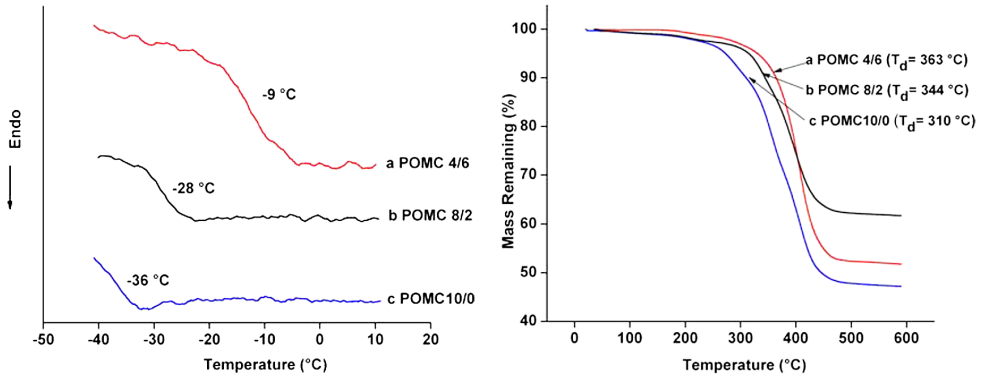

Figure 3. Thermal characterization of POMC. (A) DSC thermograph of (a) POMC4/6, (b) POMC8/2 and (c) POMC10/0 films with respective T_g at −9°C, −28°C and −36°C. (B) TGA graph of (a) POMC4/6, (b) POMC8/2 and (c) POMC10/0 films indicating the decomposition temperature (T_d, at 10% weight loss) at 363°C, 310°C and 344°C, respectively. This figure is published in colour in the online edition of this journal, that can be accessed *via* http://www.brill.nl/jbs

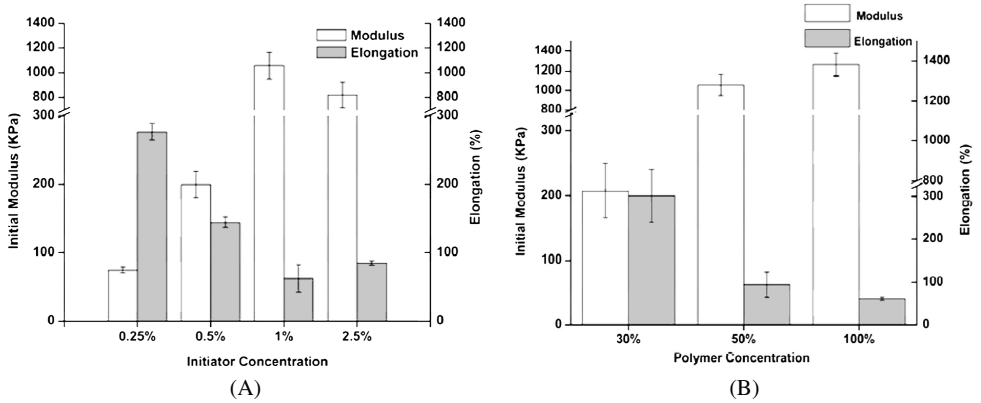

Figure 4. Mechanical properties of photo-cross-linked POMC with varying polymerization conditions. (A) Effects of concentration of photoinitiator while cross-linking prePOMC8/2 (50 wt% in DMSO) on polymer initial modulus and elongation ($n = 6$). (B) Effect of polymer concentration in DMSO while cross-linking pre-POMC8/2 with 1% of photoinitiator concentration on polymer initial modulus and elongation ($n = 6$).

(0.48 ± 0.07 MPa) was found when compared to POMC8/2 (1.06 ± 0.11 MPa). The effects of the PI and polymer concentration were also investigated. As the PI concentration increased from 0.25% to 1.0%, an increase in the initial modulus (0.07 ± 0.01 to 1.06 ± 0.11 MPa) and decrease in elongation (276.87 ± 11.7% to 62.63 ± 19.8%) was seen (Fig. 4A, $P < 0.001$). However, the PI concentration had no further effect on the initial modulus and elongation after 1.0%. Similarly, the pre-polymer concentration also affected the mechanical properties of the cross-linked material (Fig. 4B). It was observed that increasing the concentration of polymer

while cross-linking from 30% to 100% resulted in a 6-fold increase in the initial modulus (0.21 ± 0.04 MPa to 1.26 ± 0.12 MPa), and a 5-fold decrease in the elongation ($199.66 \pm 40\%$ to $40.38 \pm 2.34\%$). Furthermore, the effects of the UV cross-linking time (3–30 min) were also studied, but no significant change in ultimate strain and stress was observed (data not shown). The densities of the POMC films were calculated according to the Archimedes principle. It was observed that density decreased as the molar ratio of MA decreased, as seen in Table 2.

3.4. Swelling Properties and Sol–Gel Fraction

In order to understand the swelling behavior of the polymer, detailed studies on the effect of monomer composition, PI concentration, and pre-polymer concentration were performed. As seen in Fig. 5A, as the amount of citric acid was increased,

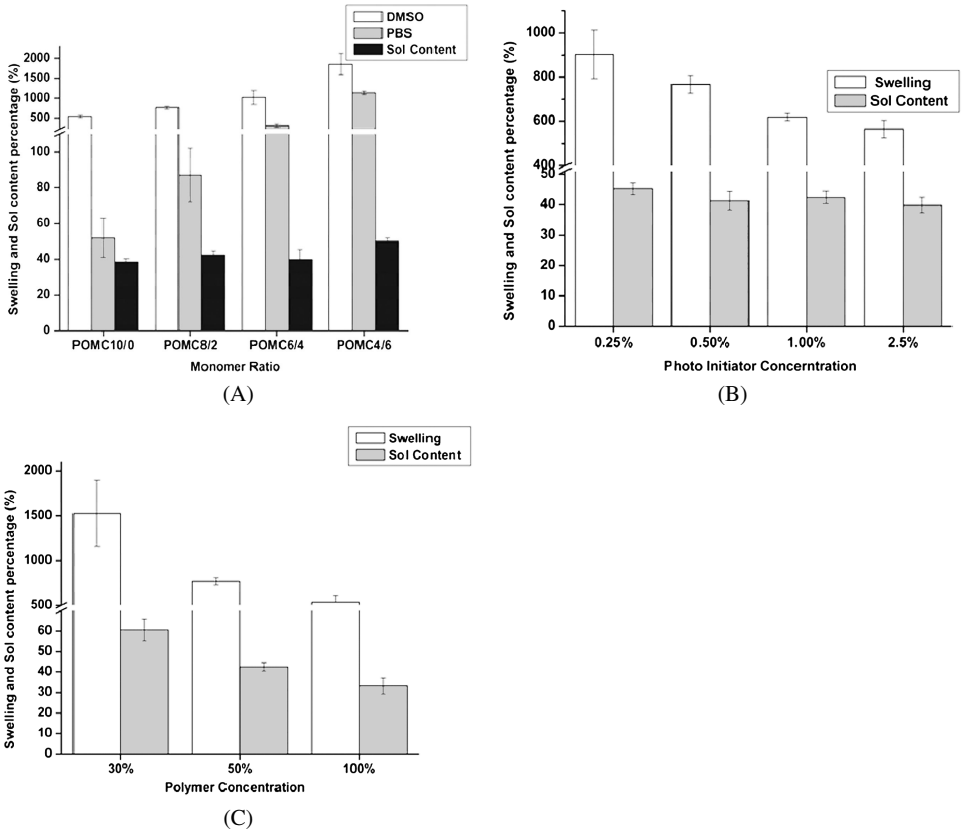

Figure 5. Swelling and sol content of photo-cross-linked POMC with varying polymerization conditions. (A) Effect of maleic acid and citric acid ratio cross-linked with 1% photoinitiator and 50% polymer in DMSO. (B) effect of concentration of photoinitiator while cross-linking pre-POMC8/2 with 50% polymer in DMSO and (C) effect of polymer concentration in DMSO while cross-linking pre-POMC8/2 with 1% photoinitiator. Swelling agents are used as DMSO and PBS. Sol content was leached out from the film in DMSO ($n = 6$).

the swelling capacity of the polymer increased in both swelling agents (DMSO and PBS). Similarly, a significant difference in the swelling behavior was observed when the PI concentration changed (Fig. 5B, $P < 0.05$). For example, the POMC films cross-linked by 0.25% PI had a swelling ratio of 903%, while the POMC films cross-linked by 1.0% PI concentration had a swelling ratio of 564% in DMSO. A significant difference was noticed on the swelling behavior when the concentration of polymer was varied (Fig. 5C, $P < 0.05$).

The sol gel fraction of the cross-linked polymer was determined by soaking freshly cross-linked polymer disks in DMSO for 2 days. As seen in Fig. 5A, as the molar ratio of MA increased and polymer concentration decreased, there is a significance decrease in the sol fraction of the polymer ($P < 0.05$). However, no significant difference in the sol–gel fraction is seen when the amount of the PI concentration is varied (Fig. 5B and 5C).

3.5. Degradation of POMC

Figure 6 shows the hydrolytic degradation rate of POMC polymer films with different monomer ratios in PBS at 37°C. As the molar ratio of MA increased, the degradation rate decreased. 70% of the polymer mass was lost within a 3 months for POMC4/6, whereas only a 10% mass loss was observed on the POMC10/0 film.

3.6. Collagen Immobilization onto POMC

When comparing the bond vibration peaks of POMC8/2 and collagen-immobilized POMC8/2 films, the appearance of a peak at 1648, 1544 and 3450 cm^{-1} correlates to amide I, amide II and amine groups, respectively. Figure 7 shows the successful introduction of amide groups to the polymer surface achieved from the immobilization of collagen.

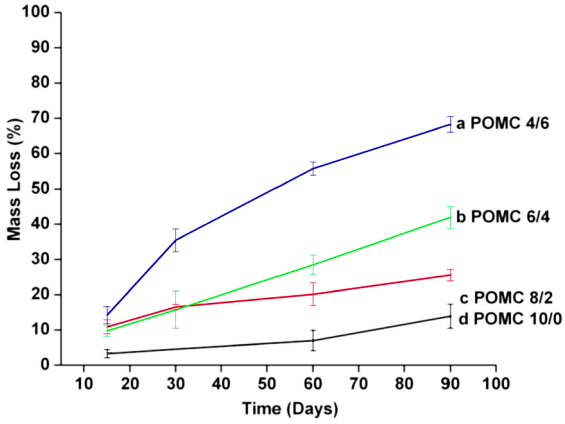

Figure 6. *In vitro* degradation of POMC in PBS (pH 7.4, 37°C). (a) POMC4/6, (b) POMC6/4, (c) POMC8/2 and (d) POMC10/0. This figure is published in colour in the online edition of this journal, that can be accessed *via* http://www.brill.nl/jbs

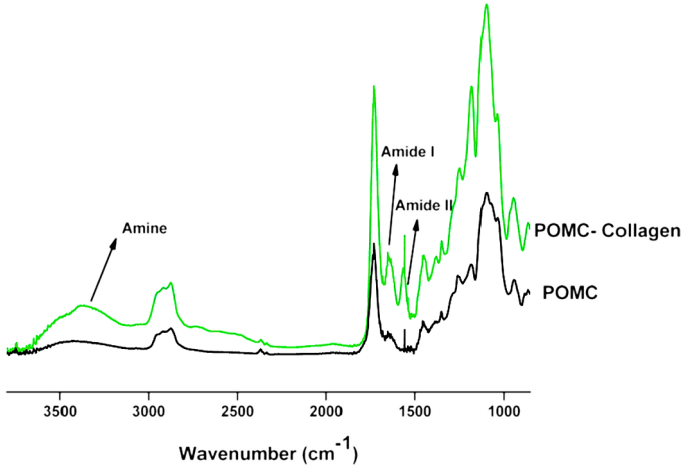

Figure 7. The FT-IR–ATR spectra of the POMC8/2 film and collagen-immobilized POMC8/2 film. Amide I, amide II and amine, representing peaks at 1648, 1544 and 3450 cm^{-1} in collagen-immobilized POMC8/2 film, illustrate the successful conjugation of collagen to POMC surface. This figure is published in colour in the online edition of this journal, that can be accessed *via* http://www.brill.nl/jbs

3.7. Cell Attachment and Foreign Body Response of POMC

After 72 h in culture, both HASMCs and NIH-3T3 fibroblast cell lines attached and proliferated on POMC and collagen-immobilized POMC films. NIH-3T3 maintained a normal and healthy spindle-shape morphology during the proliferation process on both films (Fig. 8A and 8B). Quantitative MTT analysis show that cells proliferated better on PLLA films when compared to non-collagen-immobilized POMC films. After type-I collagen immobilization, no significant difference in HASMC cell adhesion and proliferation was observed for POMC and PLLA films (Fig. 8C). These results demonstrate that our POMC hydrogel possesses a significant cell affinity even without modification. Surface modification with cell-adhesive collagen could further increase cell adhesion and proliferation.

The foreign body response of POMC was evaluated *via* subcutaneous implantation in Sprague–Dawley rats. Food and Drug Administration (FDA)-approved biodegradable polymer PLLA was used as a control. POMC and PLLA produced an comparable acute inflammatory response characterized by a cell-accumulated layer surrounding the implants after 1 week implantation which was expected and consistent with the introduction of foreign materials into body. The thickness of the cell layers are 284.29 ± 25.42 μm for POMC and 312.38 ± 20.20 μm for PLLA (Fig. 9A and 9B). After 4 weeks of implantation, the number of surrounding cells declined by 29% on POMC and 25% on PLLA and stabilized into fibrous capsules surrounding of the implants (Fig. 9C and 9D). No tissue necrosis was found throughout the *in vivo* studies.

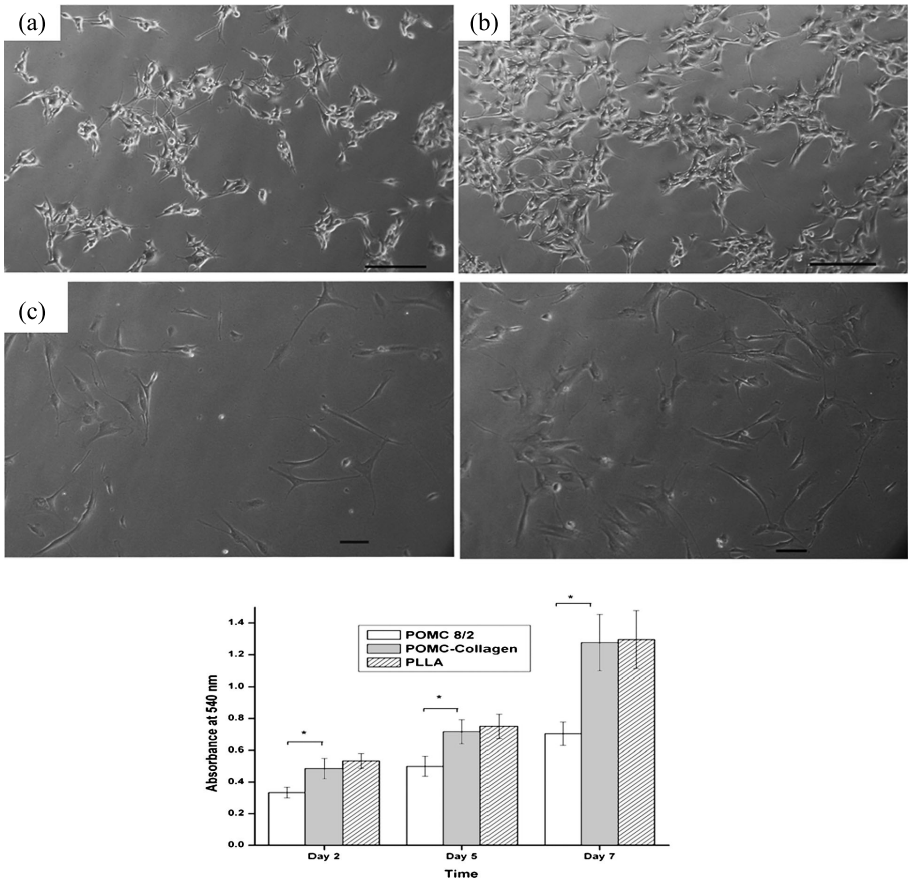

Figure 8. (a, b) Photomicrograph of NIH-3T3 cell culture for 48 h on (a) POMC8/2 film and (b) collagen-immobilized POMC8/2 film. (c, d) HASMCs cell culture for 48 h on (c) POMC8/2 film and (d) collagen-immobilized POMC8/2 film. (e) MTT assay for HASMC cell growth on POMC 8/2, collagen-immobilized POMC8/2 and PLLA control for 2, 5 and 7 days ($n = 7$), $^{*}P < 0.05$. Scale bar = 100 μm.

3.8. POMC Scaffold Fabrication and In Situ *Film Formation*

The processability of POMC was demonstrated through the fabrication of microporous scaffolds and *in situ* film formation on porcine skin cavities (data not shown). Figure 10A and 10B shows SEM pictures of the surface and the cross-section of a POMC8/2 scaffold produced using the salt leaching technique. The SEM picture indicates a porous POMC8/2 scaffold with average pore size of 100 μm.

4. Discussion

Advanced technologies such as tissue engineering, drug delivery and wound healing are fast-growing fields which place a huge need for suitable biomaterials to solve

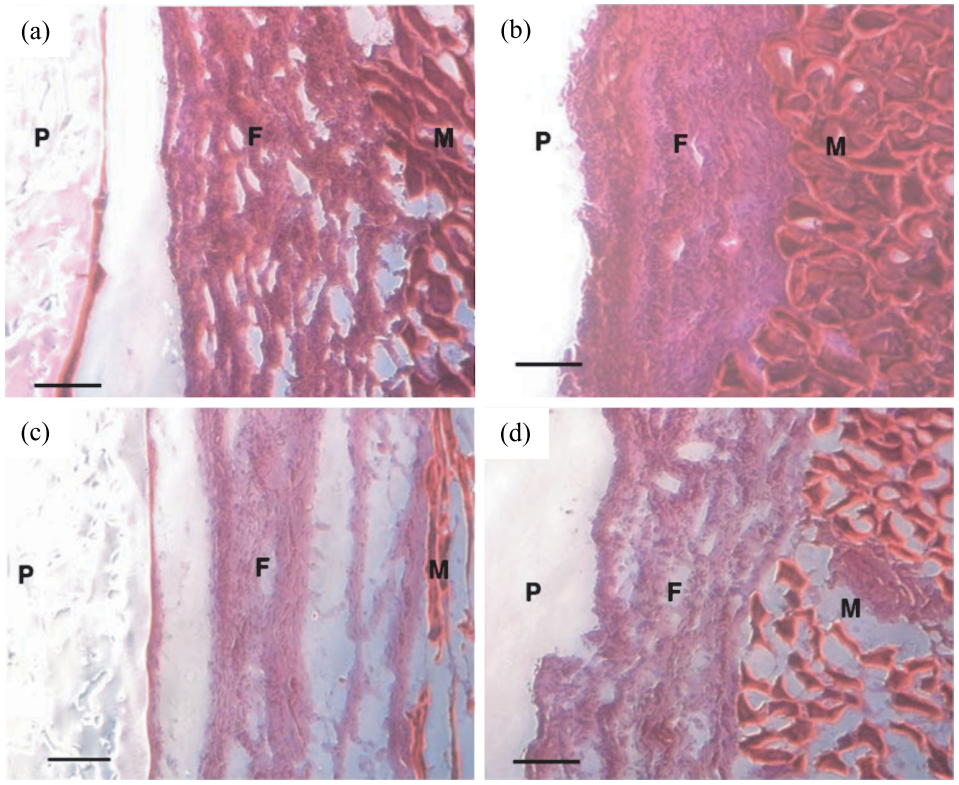

Figure 9. *In vivo* host response to photo-cross-linked POMC8/2 implanted subcutaneously in Sprague–Dawley rats. Implants and surrounding tissues were harvested 1 week after (a) POMC8/2, (b) PLLA and 4 weeks after (c) POMC8/2 and (d) PLLA implantation. No tissue necrosis was found. P, polymer; F, fibrocapsule; M, muscle. Scale bar = 100 μm. This figure is published in colour in the online edition of this journal, that can be accessed *via* http://www.brill.nl/jbs

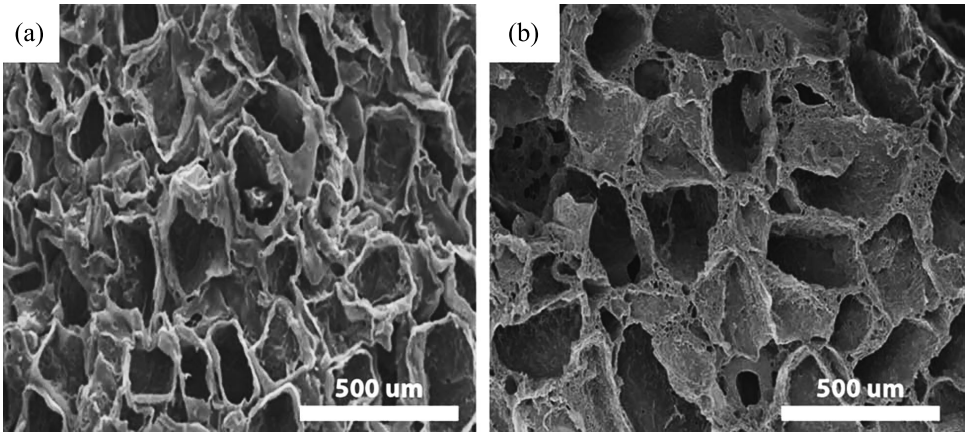

Figure 10. SEM pictures of the (a) surface and (b) cross-section of POMC8/2 scaffolds fabricated using the salt-leaching method.

unmet clinical problems. The development of an ideal *in situ* cross-linkable elastic biodegradable biomaterial has been a challenge. The objective of this study was to synthesize and characterize a new cross-linkable biodegradable synthetic elastomer that is able to preserve pendant chemistry in the bulk material after *in situ* cross-linking. The synthesis of POMC was built upon a previously well-characterized biodegradable elastomer, poly(octamethylene citrate) (POC) [9]. POC has demonstrated excellent biocompatibility and hemocompatibility both *in vitro* and *in vivo*. In addition, the tunable elastomeric mechanical properties allow POC to serve as a soft and elastic scaffold material for the engineering of vasculature [9]. The importance of matching the scaffold mechanical properties to those of the tissues has been recognized. However, the tunability of the mechanical properties of POC was achieved at the price of sacrificing the reactable functional groups in the pre-polymer backbone, thus limiting its potential for *in situ* applications and further bioconjugation. To overcome this issue, introducing a vinyl component into the backbone of POC would confer *in situ* cross-link ability to POMCs without using any harsh processing conditions or sacrificing the available functional groups. This new approach to cross-link the polymer network will open new windows for broader biomedical applications in which biodegradable elastomers are needed.

The synthesis of POMCs is easy, simple and inexpensive. The polycondensation reaction between CA, OD and MA was driven forward by removal of water through the addition of heat. In order to prepare a linear pre-polymer of lower molecular mass, the reaction was subjected to heat for limited amount of time. Introduction of MA in the pre-polymer provided double bonds that can be utilized in the formation of C–C bonds *via* exposure to UV light. The tri-functional citric acid contributes the excess pendent carboxylic and hydroxyl group in the polymeric backbone. The ester linkages of the polyester polymers confer biodegradability to the polymers [43]. The aliphatic diol, 1,8-octanediol, was used to balance the hydrophilicity and also participated in the ester bond formation.

The compositions of the polymer determined by ^{1}H-NMR was found to be consistent with the feed ratios as seen in Table 1. Thus, all the monomers participated in the reaction as expected. ^{1}H-NMR also shows two different pairs of vinyl hydrogen peaks between 6 and 7 ppm. This suggests that maleic acid has been incorporated into the polymeric chain in two different environments. This can be explained with the concept of the first and second acid dissociation constant (pK_a) values for both acids. The first pK_a values of MA and CA are 1.97 and 3.15, and the second pK_a values are 6.07 and 4.77, respectively. As both of the acids need to take part in the reaction, the lower second pK_a value of the CA will render CA more reactive than MA, which increases the chance for polymer chain termination with MA.

Similarly, the FT-IR spectra in Fig. 2C confirmed the presence of all the characteristic bonds, such as ester, double and hydrogen-bonded hydroxyl groups, that contribute to the biocompatibility, hydrophilicity, degradability, thermal and mechanical properties of the materials [46]. As compared to the FT-IR spectra of the reported POC synthesized from citric acid and 1,8-octanediol [8], an additional peak

at 1650 cm^{-1} of pre-POMC suggested that MA was incorporated in the chain of the pre-polymer. The double bond peak at 1650 cm^{-1} significantly decreases when pre-POMC is subjected to UV cross-linking. The peaks centered at 3750 cm^{-1} on both pre-polymers and photo-cross-linked films indicate that –COOH and –OH groups were preserved, which are essential for potential bioconjugation.

The typical DSC thermograph (Fig. 3A) showed a T_g below 0°C for all polymers, along with the absence of any crystallization and melting peaks. This property allowed all polymers to maintain an amorphous state at room or body temperature which is characteristic for elastomers [47]. As the amount of MA in the polymers increased, the T_g of the polymers further decreased. This was due to the presence of isolated double bonds which facilitates polymer to move freely even in lower temperatures. In addition, as the amount of MA increased, the amount of CA decreased, which reduced the amount of hydrogen bonding that is responsible for polymer chain immobility. It can be concluded from the TGA analysis that this material has better thermal stability and lower T_d than POC.

One of the prime interests in developing biodegradable elastomers with soft and elastic properties to match the mechanical properties of soft tissues [2, 9, 33, 46, 47] such as myocardium of human (tensile strength 3–15 kPa; modulus 0.02–0.5 MPa) [10], stratum corneum of human skin (breaking threshold of 20–40 kPa) [48] and human bladder (tensile strength 0.27 ± 0.14 MPa; modulus 0.25 ± 0.18 MPa) [46]. The mechanical properties of these soft tissues fall within the range of the POMC mechanical properties, which can be tuned by varying the molar ratio of the monomers, the amount of PI used and concentration of polymer. For example, a very soft and elastic polymer can be obtained by using lower initiator concentrations, lower polymer concentrations and a higher molar ratio of CA. In contrast, a tougher elastomer can be obtained by using higher initiator concentrations, higher polymer concentrations and a higher molar ratio of MA.

It should be noted that if citric acid is not present in the polymeric network, there is a significant decrease in the ultimate tensile strength of the polymer. This explains that the strong hydrogen bonding between carboxylic acid and hydroxyl contribute to the strength of the elastomer. Another interesting observation was that the polymer increased its stiffness and strength if initiator concentration was increased from 0.25% to 1%, whereas the trend was disrupted when the initiator was increased to 2.5%. This may explain that the increased initiator concentration from 0.25% to 1% resulted in increased cross-linking degree, which in turn resulted in increased initial modulus and decreased elongation. However, when the concentration of initiator is higher than 1%, the free radical polymerization terminated with short polymer chains due to excess of radicals, which resulted in loss of stiffness of the polymer.

In addition, the elastic mechanical properties of the polymer can potentially be further modulated by changing the choice of the diol (aliphatic diols such as C2–C12 diols and macrodiols such as poly(ethylene glycol) (PEG) of varying molecular mass). The use of PEG for the polymer synthesis can make the polymers

water-soluble (data not shown). Thus, many different methods can be combined to fine tune the mechanical properties of the resulting polymer to fit a specific application.

As the CA content in the polymer was increased, the swelling ratio trend of POMC was more drastic in PBS than in DMSO. This can be explained by the increase in the amount of CA in the polymer network providing more available –COOH. The free carboxylic acid pendant groups can be ionized in PBS to charge the polymer chains, causing repulsion among the polymer chains, which resulted in higher swelling ratios. A similar observation was made in the degradation study. The degradation was accelerated with the increased amount of hydrophilic CA due to the easier access of water to the polymer network. The polymer absorbed more fluid as the amount of CA increases, thus creating more chances for the ester bond to be degraded by hydrolysis.

The preliminary cytocompatibility evaluations performed with POMC films *in vitro* showed that both HASMCs and 3T3 fibroblasts display a typical spindle-shape morphology on POMC films. Supporting cell adhesion is the first step to demonstrate the utility of a material for tissue-engineering applications. When implanted *in vivo*, the polymers did not trigger edema and tissue necrosis on all the tested animals. Although, a slight acute inflammation response was observed in the first week of the implantation, the number of surrounding cells declined reducing the fibrous capsule around the sample at the 4th week of implant. This may suggest that degradation products of POMCs were not toxic to produce any tissue death and is comparable to PLLA. Detailed biocompatibility tests of all POMC polymers will be the topic of future publications.

One major benefit of POMC is that the polymer remains saturated with pendant functionalities after *in situ* cross-linking. Cellular adhesion and proliferation on un-modified POMC films produced poor results, which could be expected from the functionally rich surface of the material and is similar to the results of other studies [49]. However, type-I collagen-modified POMC films showed a significant increase in the cellular proliferation, and was comparable to the cellular response on PLLA films. Unlike previous elastomers, no further post-modifications are required to introduce functional groups, which may alter the properties of the material. The conjugation for POMC is convenient and can be performed in the bulk of the material. The un-reacted carboxylic acid and hydroxyl groups on the POMC backbone can potentially be used as bioconjugation sites if proteins, drugs, peptides and ligands are needed to confer biological functions to the materials [50–55].

The processability of POMC was demonstrated by the fabrication of microporous 3-D scaffolds. We have demonstrated that POMC could be fabricated into a 3-D tissue-engineering scaffold using the commonly used particulate leaching technique (Fig. 10). The low molecular mass (low viscosity) of pre-POMC can itself be used without use of organic solvent that potentially makes POMC potential for *in situ* applications. Pre-POMC can be smeared on the skin to conform to any contour and quickly form a thin film *in situ*, thus rendering this material potential for *in*

situ applications such as *in situ* forming wound dressing and drug-delivery application. POMCs can be made into water-soluble by replacing or partially replacing the relatively hydrophobic 1,8-octanediol with hydrophilic PEG in the syntheses. Water-soluble pre-polymer can be cross-linked with photo or redox initiators to further expand the *in situ* applications where the materials are injected into the body with cells or drugs. Our lab is actively studying water-soluble POMC for *in situ* tissue engineering and drug-delivery applications.

5. Conclusion

In this work, we have synthesized and evaluated a new class of photo-cross-linkable synthetic biodegradable elastomeric polyester. The material properties including mechanical properties, degradation, thermal, swelling properties of POMC films can be tuned through the monomer ratios, polymer concentration and initiator concentration. POMC films support cell adhesion and proliferation demonstrating its potential serving as scaffolding materials in soft tissue engineering. The pendant chemistry of cross-linked POMC facilitates the further bioconjugation for enhanced biocompatibility, exemplified by collagen conjugation. POMC films also demonstrate favorable *in vivo* host responses. The development of POMC enriches the family of CA-derived biodegradable elastomers and expands the available biodegradable polymers for versatile needs in biomedical applications.

Acknowledgements

This work was supported in part by Beginning Grant-in-Aid award (to J.Y.) from the American Heart Association (AHA), and award R21EB009795 (to J.Y.) from the National Institute of Health/National Institute of Biomedical Imaging and Bioengineering (NIH/NIBIB).

References

1. J. P. Bruggeman, B. J. de Bruin, C. J. Bettinger and R. Langer, *Biomaterials* **29**, 4726 (2008).
2. Y. Wang, G. A. Ameer, B. J. Sheppard and R. Langer, *Nature Biotechnol.* **20**, 602 (2002).
3. H. M. Younes, E. Bravo-Grimaldo and B. G. Amsden, *Biomaterials* **25**, 5261 (2004).
4. J. Y. Shen, X. Y. Pan, C. H. Lim, M. B. Chan-Park, X. Zhu and R. W. Beuerman, *Biomacromolecules* **8**, 376 (2007).
5. X. Huang, C. C. Li, L. C. Zheng, D. Zhang, G. H. Guan and Y. N. Xiao, *Polym. Int.* **58**, 893 (2009).
6. J. J. Guan, J. J. Stankus and W. R. Wagner, *Cell Transplant.* **15**, S17 (2006).
7. A. Jacinto, A. Martinez-Arias and P. Martin, *Nature Cell Biol.* **3**, E117 (2001).
8. Y. Kang, J. Yang, S. Khan, L. Anissian and G. A. Ameer, *J. Biomed. Mater. Res.* **77A**, 331 (2006).
9. J. Yang, A. R. Webb, S. J. Pickerill, G. Hageman and G. A. Ameer, *Biomaterials* **27**, 1889 (2006).
10. Q. Z. Chen, A. Bismarck, U. Hansen, S. Junaid, M. Q. Tran, S. E. Harding, N. N. Ali and A. R. Boccaccini, *Biomaterials* **29**, 47 (2008).
11. A. K. Shung, M. D. Timmer, S. B. Jo, P. S. Engel and A. G. Mikos, *J. Biomater. Sci. Polymer Edn* **13**, 95 (2002).

12. S. A. Zawko, S. Suri, Q. Truong and C. E. Schmidt, *Acta Biomater.* **5**, 14 (2009).
13. S. J. Bryant, J. A. Arthur and K. S. Anseth, *Acta Biomater.* **1**, 243 (2005).
14. D. M. Brey, J. L. Ifkovits, R. I. Mozia, J. S. Katz and J. A. Burdick, *Acta Biomater.* **4**, 207 (2008).
15. W. E. Hennink and C. F. van Nostrum, *Adv. Drug Deliv. Rev.* **54**, 13 (2002).
16. R. G. Payne, M. J. Yaszemski, A. W. Yasko and A. G. Mikos, *Biomaterials* **23**, 4359 (2002).
17. J. S. Temenoff and A. G. Mikos, *Biomaterials* **21**, 2405 (2000).
18. R. A. Stile and K. E. Healy, *Biomacromolecules* **2**, 185 (2001).
19. M. P. Lutolf and J. A. Hubbell, *Biomacromolecules* **4**, 713 (2003).
20. K. T. Nguyen and J. L. West, *Biomaterials* **23**, 4307 (2002).
21. J. D. Kretlow, L. Klouda and A. G. Mikos, *Adv. Drug Deliv. Rev.* **59**, 263 (2007).
22. J. L. Ifkovits and J. A. Burdick, *Tissue Eng.* **13**, 2369 (2007).
23. Q. P. Hou, D. W. Grijpma and J. Feijen, *Acta Biomater.* **5**, 1543 (2009).
24. B. G. Amsden, G. Misra, F. Gu and H. M. Younes, *Biomacromolecules* **5**, 2479 (2004).
25. Q. P. Hou, P. A. De Bank and K. M. Shakesheff, *J. Mater. Chem.* **14**, 1915 (2004).
26. A. Khademhosseini, G. Eng, J. Yeh, J. Fukuda, J. Blumling, R. Langer and J. A. Burdick, *J. Biomed. Mater. Res.***79A**, 522 (2006).
27. Y. Du, E. Lo, S. Ali and A. Khademhosseini, *Proc. Natl. Acad. Sci. USA* **105**, 9522 (2008).
28. A. Hatefi and B. Amsden, *J. Control. Rel.* **80**, 9 (2002).
29. C. L. Nijst, J. P. Bruggeman, J. M. Karp, L. Ferreira, A. Zumbuehl, C. J. Bettinger and R. Langer, *Biomacromolecules* **8**, 3067 (2007).
30. S. Gerecht, S. A. Townsend, H. Pressler, H. Zhu, C. L. E. Nijst, J. P. Bruggeman, J. W. Nichol and R. Langer, *Biomaterials* **28**, 4826 (2007).
31. R. T. Tran, Y. Zhang, D. Gyawali and J. Yang, *Recent Pat. Biomed. Eng.* **2**, 216 (2009).
32. H. J. Qiu, J. Yang, P. Kodali, J. Koh and G. A. Ameer, *Biomaterials* **27**, 5845 (2006).
33. J. Yang, A. R. Webb, G. Hageman and G. A. Ameer, *Adv. Mater.* **16**, 511 (2004).
34. J. Yang, D. Motlagh, A. R. Webb and G. A. Ameer, *Tissue Eng.* **11**, 1876 (2005).
35. J. Dey, H. Xu, J. H. Shen, P. Thevenot, S. R. Gondi, K. T. Nguyen, B. S. Sumerlin, L. P. Tang and J. Yang, *Biomaterials* **29**, 4637 (2008).
36. J. Yang, Y. Zhang, S. Gautam, L. Liu, J. Dey, W. Chen, R. P. Mason, C. A. Serrano, K. A. Schug and L. Tang, *Proc. Natl. Acad. Sci. USA* **106**, 10086 (2009).
37. J. P. Bruggeman, C. J. Bettinger, C. L. E. Nijst, D. S. Kohane and R. Langer, *Adv. Mater.* **20**, 1922 (2008).
38. J. Yang, D. Motlagh, J. B. Allen, A. R. Webb, M. R. Kibbe, O. Aalami, M. Kapadia, T. J. Carroll and G. A. Ameer, *Adv. Mater.* **18**, 1493 (2006).
39. K. Amoa, *J. Chem. Educ.* **84**, 1948 (2007).
40. J. Daruwalla, K. Greish, C. Malcontenti-Wilson, V. Muralidharan, A. Iyer, H. Maeda and C. Christophi, *J. Vasc. Res.* **46**, 218 (2008).
41. Y. Lu and N. S. Mosier, *Biotechnol. Bioeng.* **101**, 1170 (2008).
42. T. W. Wong, S. Wahab and Y. Anthony, *Int. J. Pharm.* **357**, 154 (2008).
43. C. J. Bettinger, J. P. Bruggeman, J. T. Borenstein and R. S. Langer, *Biomaterials* **29**, 2315 (2008).
44. E. Behravesh, A. K. Shung, S. Jo and A. G. Mikos, *Biomacromolecules* **3**, 153 (2002).
45. S. Kaihara, S. Matsumura and J. P. Fisher, *Eur. J. Pharm. Biopharm.* **68**, 67 (2008).
46. A. R. Webb, J. Yang and G. A. Ameer, *Expert. Opin. Biol. Ther.* **4**, 801 (2004).
47. H. M. Younes, E. Bravo-Grimaldo and B. G. Amsden, *Biomaterials* **25**, 5261 (2004).
48. L. Pedersen and G. B. Jemec, *Acta. Derm. Venereol.* **86**, 308 (2006).
49. Y. Q. Wan, G. Feng, F. H. Shen, G. Balian, C. T. Laurencin and X. D. Li, *Macromol. Biosci.* **7**, 1217 (2007).

50. P. X. Ma, *Adv. Drug Deliv. Rev.* **60**, 184 (2008).
51. J. Yang, J. Bei and S. Wang, *Biomaterials* **23**, 2607 (2002).
52. M. Fujita, B. S. Lee, N. M. Khazenzon, M. L. Penichet, K. A. Wawrowsky, R. Patil, H. Ding, E. Holler, K. L. Black and J. Y. Ljubimova, *J. Control. Rel.* **122**, 356 (2007).
53. W. J. Duncanson, M. A. Figa, K. Hallock, S. Zalipsky, J. A. Hamilton and J. Y. Wong, *Biomaterials* **28**, 4991 (2007).
54. S. H. Hsu, S. W. Whu, S. C. Hsieh, C. L. Tsai, D. C. Chen and T. S. Tan, *Artif. Organs* **28**, 693 (2004).
55. S. E. Sakiyama-Elbert and J. A. Hubbell, *Annu. Rev. Mater. Res.* **31**, 183 (2001).